Supplementary Materials for

Harnessing highly efficient coherent polariton parametric emission in quantum confined perovskite microcavities

Xinyi Deng[1]†, Sanjib Ghosh[2]†, Jiepeng Song[1], Chengyong Yu[2], Chun Li[1], Xinfeng Liu[3]*, Qing Zhang[1]*

[1]School of Materials Science and Engineering, Peking University, Beijing 100871, P.R. China

[2]School of Science and Engineering, The Chinese University of Hong Kong, Shenzhen, Shenzhen 518172, P.R. China

[3]CAS Key Laboratory of Standardization and Measurement for Nanotechnology, National Center for Nanoscience and Technology, Beijing 100190, P.R. China

†These authors contributed equally: Xinyi Deng and Sanjib Ghosh.

*Corresponding author. Email: q_zhang@pku.edu.cn; liuxf@nanoctr.cn

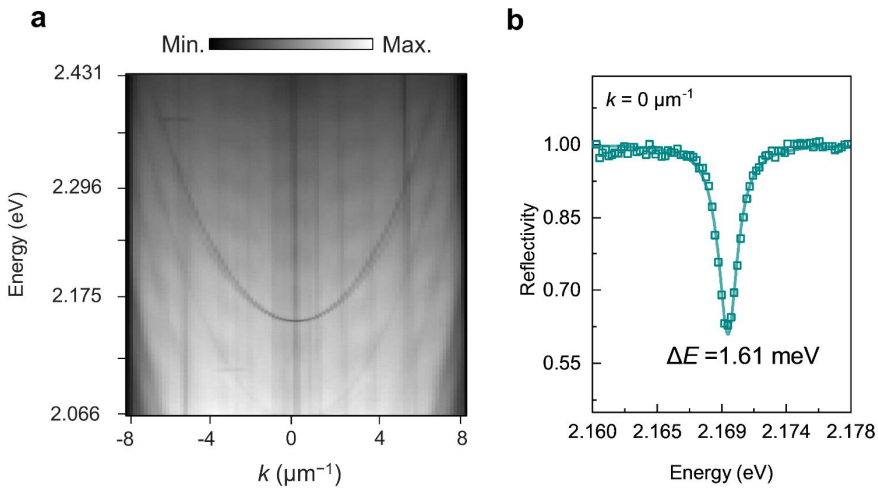

Figure S1. Cavity quality. (a) Angle-resolved reflectivity of the empty cavity. (b) Extracted reflection spectrum at 0 μm^{-1} from (a), showing a linewidth of 1.61 meV and Q factor of ~1300.

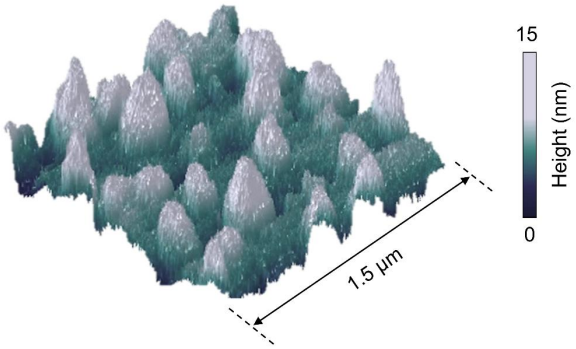

Figure S2. Atomic force microscopr (AFM) measured surface morphology of a $CsPbBr_3$ microplatelet after PDMS dry transfer. Pseudo-colors denote height profile.

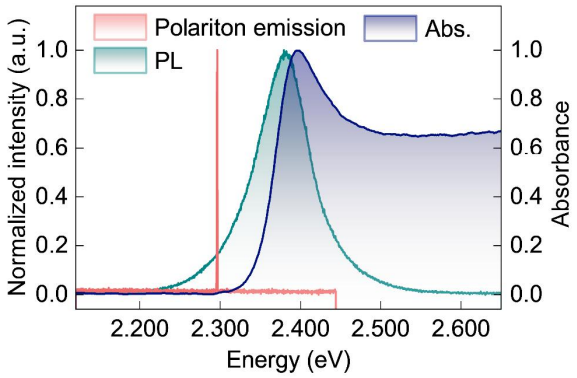

Figure S3. Absorbance (blue), and photoluminescence (green) of bare $CsPbBr_3$ microplate. And polariton condensate emission in a $CsPbBr_3$ microcavity.

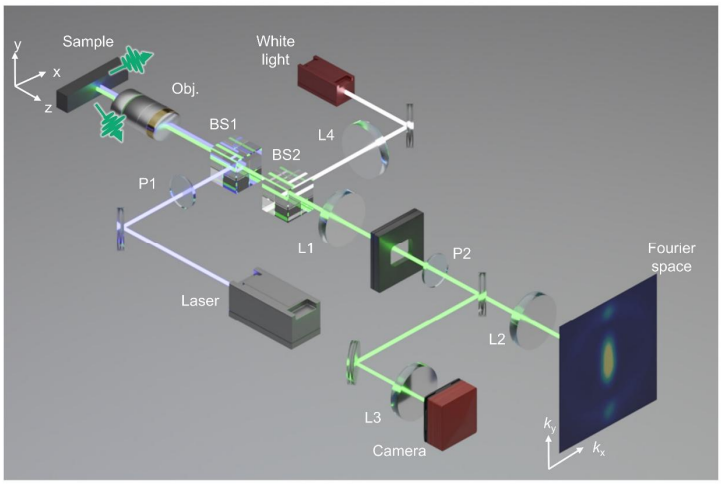

Figure S4. Schematic diagram of the angle-resolved setup for measurement of polariton parametric scattering in a trapped microcavity. Microplatelet sample direction (gray cube in upper left corner) and respective signal and idler polariton (green arrows near the sample, and bright high-k spots in Fourier space) are depicted. (Obj: objective, L: lens, P: polarizer, BS: beam splitter)

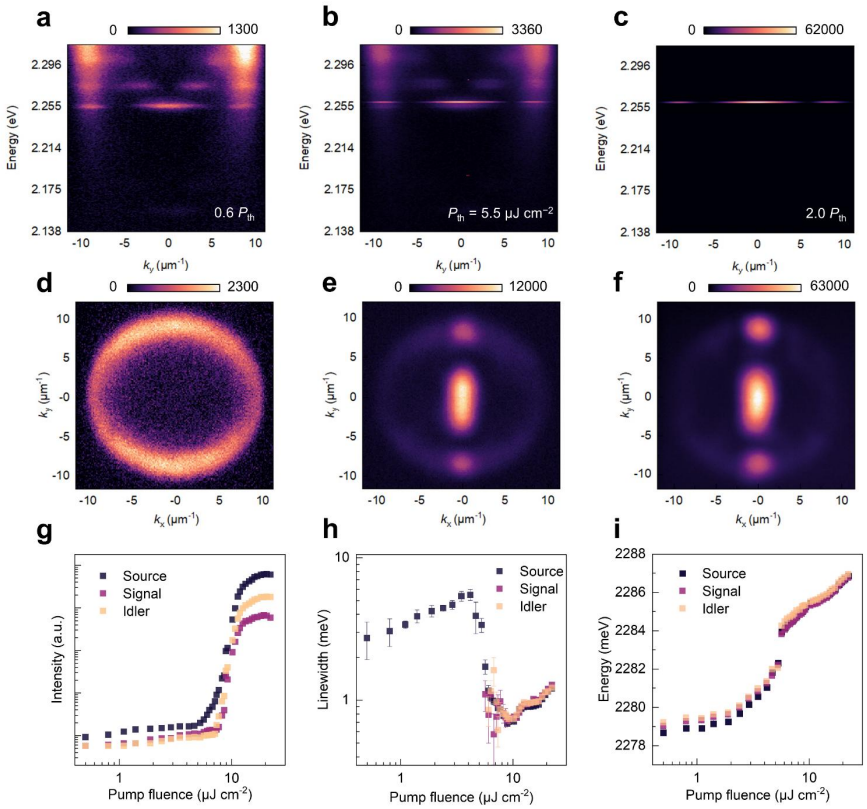

Figure S5. Power dependent analysis of polariton condensation and parametric scattering. (a-c) Angle-resolved photoluminescence spectra under pulsed excitation at $0.6P_{th}$, P_{th}, and $2P_{th}$, respectively. (d-f) Momentum space emission corresponding to (a-c). (g-h) Extracted pump fluence dependent intensity the source, signal and idler polaritons, respectively. (h) Pump fluence dependent linewidth. (i) Pump fluence dependent energy blueshift.

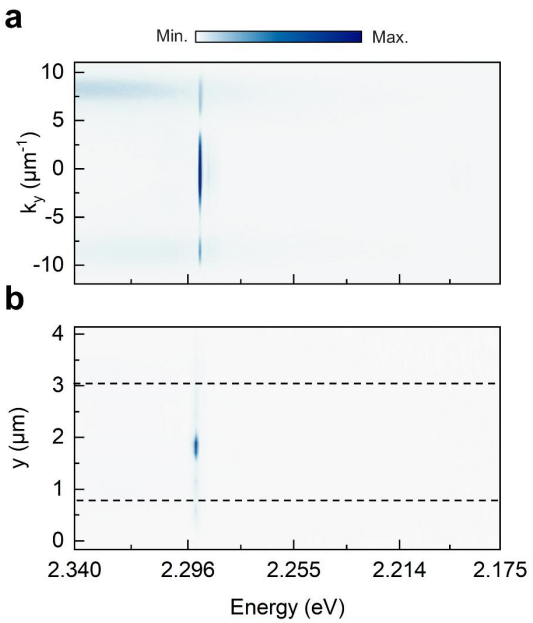

Figure S6. Comparison of the parametric emission in momentum (b) and coordinate space (a), above condensation threshold. Black dashed lines highlight the real space edge of the sample.

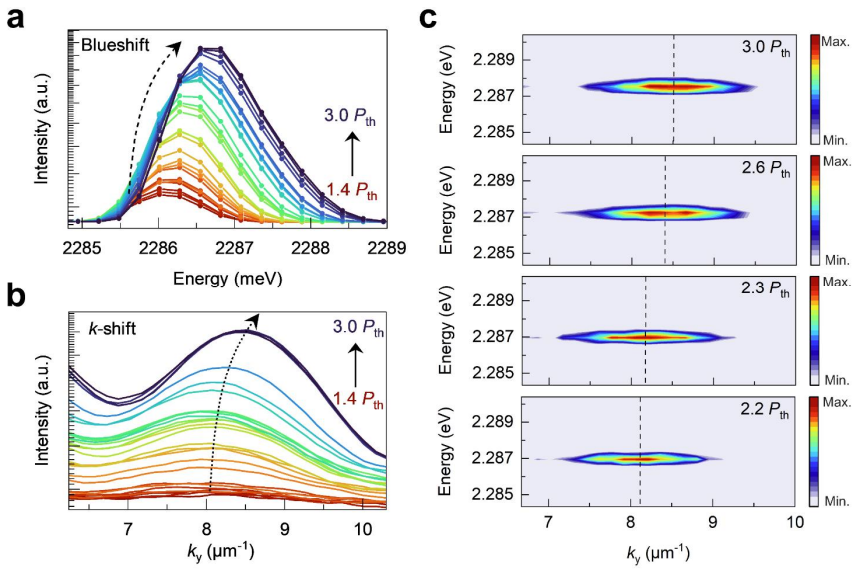

Figure S7. Blueshift-dependent wavevector change. (a) Energy-resolved spectra at 'signal' position with increasing pump fluence. (g) Wavevector-resolved 'spectra' extracted at energy position in (a), showing a shift in wavevector towards larger values. (c) Zoomed-in ARPL emission of 'idler' at four different pump densities, with black solid line as reference to highlight relative wavevector shift.

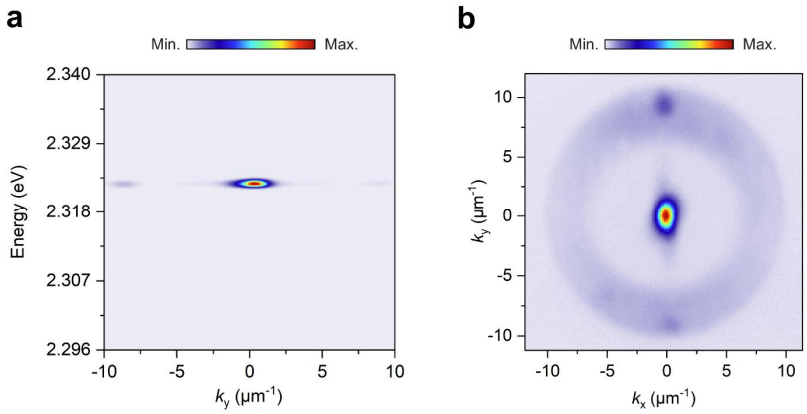

Figure S8. Parametric scattering in a non-confined planar microcavity. (a) Angle-resolved photoluminescence spectra. (b) k-space image of parametric scattering corresponding to (a).

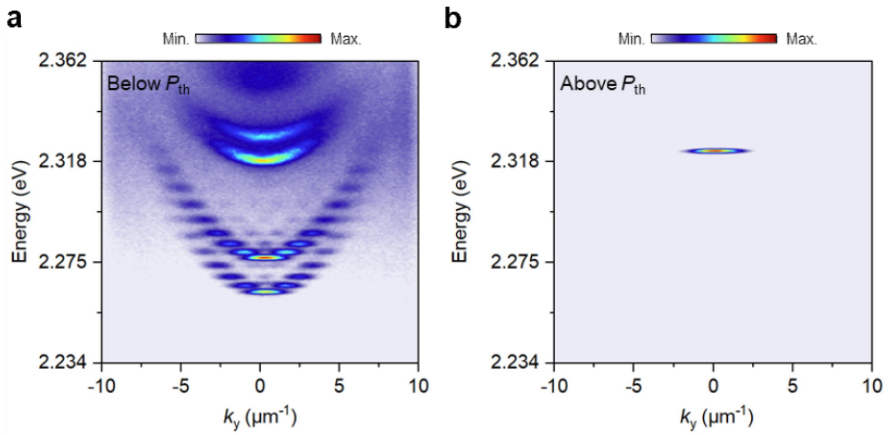

Figure S9. Polariton condensation in an in-plane confined microcavity without surface disorder, where parametric emission is absent. (a) Below condensation threshold. (b) Above condensation threshold.

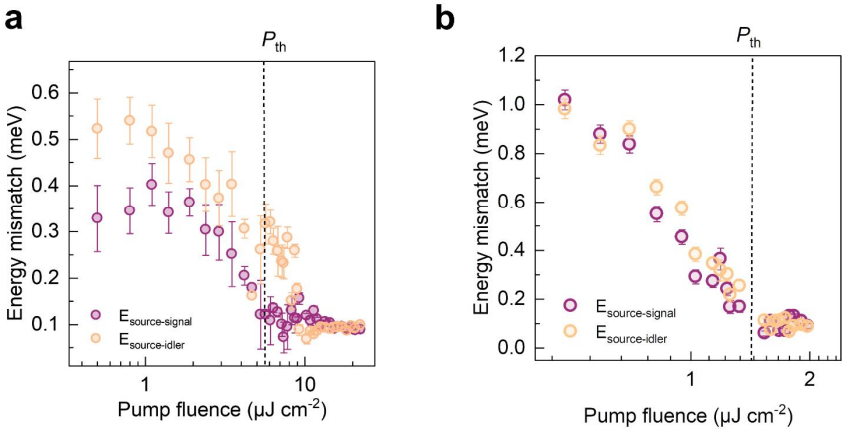

Figure S10. Energy position mismatch for source/signal, source/idler, as a function of pump fluence, for (a) Figure S5 sample, and (b) other sample. Black dashed line highlights condensation threshold. A gradual decrease in the energy mismatch is observed.

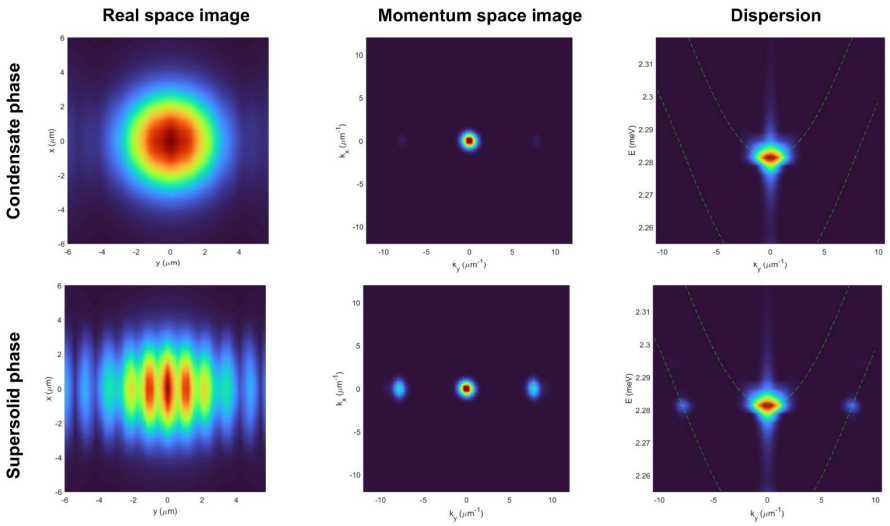

Figure S11. Theoretically simulated supersolid phase. Upper panels show the respective real space image, momentum space image, and dispersion of a polariton condensate. Lower panels show the respective results for a parametric oscillator, demonstrating formation of the supersolid phase.

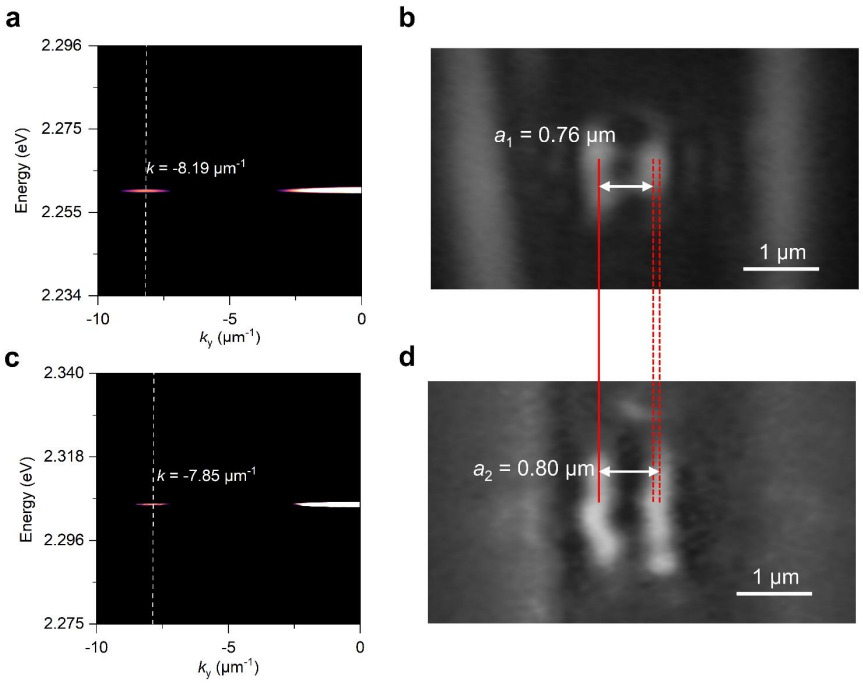

Figure S12 Supersolidity in strongly confined microcavities. (a) Angle-resolved PL spectra of parametric oscillator with signal/idler centered around k_1 = -8.19 μm^{-1}. (b) real space image of the parametric oscillator with fringes, showing fringe spacing a_1 = 0.76 μm, corresponding to momentum space of parametric emission in (a). (c) Angle-resolved PL spectra of parametric oscillator with signal/idler centered around k_1 = -7.85 μm^{-1}. (d) real space image of the parametric oscillator with with fringes, showing fringe spacing a_2 = 0.80 μm, corresponding to momentum space of parametric emission in (c).

Supplementary Note 1: Theoretical model and simulation parameters

In our theoretical model we have considered the following dispersion for the lower polariton branches:

$$E_n^{LP}(k) = \frac{\left[E_n^{cav}(k) + E_{ex} - \sqrt{(E_{cav}(k) - E_{ex})^2 + \Omega^2}\right]}{2}$$

The dispersion relations for the pure cavity modes are given by, $E_n^{cav}(k) = E_n(0) + \frac{\hbar^2}{2m_{cav}}k^2$, where $E_n(0)$ is a constant energy shift which is taken different for different cavity modes. In our simulations, we have considered two cavity modes with $n = 1$ and $n = 2$. The energy separation between the modes is considered $E_2(0) - E_1(0) = 40\ meV$. The effective mass of each cavity mode m_{cav} is approximately considered the same. In our simulation, we have considered the following parameters:

Rabi splitting $\Omega = 116\ meV$, detuning between the cavity mode and the first cavity mode is $70\ meV$. System sizes are varied as mentioned in the main text. For Figure S11 the system size is taken as $12 \times 12\ \mu m^2$. The disorder potential is considered as a random Gaussian distribution with a standard deviation $V_0 = 0.1\ meV$. The effective mass of the cavity modes $m_{cav} = 4 \times 10^{-5} m_e$ (where m_e is the electron mass), nonlinear decay $\Gamma = 0.6\ meV/\mu m^2$, nonlinear interaction $\alpha = 0.15\ meV/\mu m^2$, and the decay rate $\gamma = 0.5\ meV$. For the effective gain profile, we have considered a gaussian spot of $2.5\ \mu m$ width in both x and y directions.

The emergence of spatial modulation in the supersolid phase in a coherent parametric oscillator can be approximately understood from an effective 3 mode approximation. As can be seen from the momentum space image of the supersolid phase in Figure S11, the effective emission is coming from the 3 modes, the condensate phase with zero momentum $\psi_c = A_c$, the signal $\psi_s = A_s\, e^{-ik_0 y}$ and the idler $\psi_i = A_i e^{ik_0 y}$. Thus, the total wavefunction is given by the superposition between all three components. However, the superposition can only be ensured by the coherence between the signal and idler, which have been proven experimentally in the main text. Given the coherence between all three components, the effective wave function is given by,

$$\psi = \psi_c + \psi_i + \psi_s$$

From the momentum space image, we also confirm the symmetry between the idler and the signal implying $|\psi_i| = |\psi_s|$ ensuring $|A_i| = |A_s|$. With all these, we find that the density representing the supersolid phase is given by,

$$n(r) = |\psi(r)|^2 = |A_c|^2 + 4|A_s|^2 \cos^2 k_0 y + 4\,[Re(A_s)Re(A_c) + Im(A_s)Im(A_c)] \cos k_0 y$$

We can see the density modulation in $n(r)$ along the y axis due to the cosine function in the above expression. The density modulation comes from the coherent interference between the idler and signal creating a standing wave on top of the condensate.